THE JOURNAL OF PHYSICAL CHEMISTRY B
A JOURNAL OF THE AMERICAN CHEMICAL SOCIETY

pubs.acs.org/JPCB

Article

Comparative Study of Uracil Excited-State Photophysics in Water and Acetonitrile via RMS-CASPT2-Driven Quantum-Classical Trajectories

Published as part of The Journal of Physical Chemistry B virtual special issue "Roland Lindh Festschrift".

Meseret Simachew Bezabih, Danil S. Kaliakin,* Alejandro Blanco-González, Leonardo Barneschi, Alexander N. Tarnovsky, and Massimo Olivucci*

Cite This: *J. Phys. Chem. B* 2023, 127, 10871−10879

Read Online

ACCESS | Metrics & More | Article Recommendations | Supporting Information

ABSTRACT: We present a nonadiabatic molecular dynamics study of the ultrafast processes occurring in uracil upon UV light absorption, leading to electronic excitation and subsequent nonradiative decay. Previous studies have indicated that the mechanistic details of this process are drastically different depending on whether the process takes place in the gas phase, acetonitrile, or water. However, such results have been produced using quantum chemical methods that did not incorporate both static and dynamic electron correlation. In order to assess the previously proposed mechanisms, we simulate the photodynamics of uracil in the three environments mentioned above using quantum-classical trajectories and, for solvated uracil, hybrid quantum mechanics/molecular mechanics (QM/MM) models driven by the rotated multistate complete active space second-order perturbation (RMS-CASPT2) method. To do so, we exploit the gradient recently made available in OpenMolcas and compare the results to those obtained using the complete active space self-consistent field (CASSCF) method only accounting for static electron correlation. We show that RMS-CASPT2 produces, in general, a mechanistic picture different from the one obtained at the CASSCF level but confirms the hypothesis advanced on the basis of previous ROKS and TDDFT studies thus highlighting the importance of incorporating dynamic electron correlation in the investigation of ultrafast electronic deactivation processes.

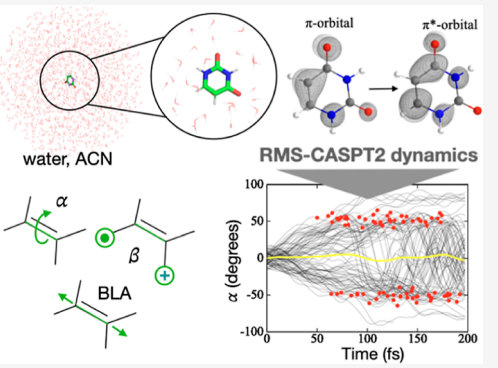

INTRODUCTION

Ultraviolet (UV) light absorption in nucleic acids is responsible for the photochemical transformations leading to mutagenesis in cells[1−7] as well as damage to any natural and synthetic material exploiting the electronic and geometrical properties of these biopolymers.[8−10] These processes are largely prevented by the existence of photoprotective ultrafast nonradiative decay channels that effectively convert the harmful electronic excitation energy into heat.[11−17] However, in spite of the many reported experimental and theoretical studies, the mechanisms of such nonadiabatic events are still blurred. This is why in the present paper we re-examine, using contemporary wave function-based multistate multiconfigurational quantum chemistry and quantum-classical trajectories, the decay channels of uracil,[7,18−54] their dynamics, and their sensitivity to the solvent. To do so we exploit potential energy gradients that have been made available only recently in OpenMolcas.[55]

The mechanistic details of UV light absorption and subsequent nonradiative decay in uracil depend on whether these processes occur in the gas phase or in solution.[38,42−45] Accordingly, the theoretical/computational description of water solvation on ground and excited states requires not only the explicit treatments of hydrogen bonds between uracil and a selected set of water molecules but also accounting for larger solvent regions.[27,32,33,36,37,39,46−48,56] Additionally, the simulation of uracil photophysics requires, in principle, a quantum chemical method accounting for both static and dynamic electron correlation as methods that lack dynamic electron correlation such as the complete active space self-consistent field (CASSCF) generate a different electronic state ordering.[32,37,48] At the same time, the computationally convenient time-dependent density functional theory (TDDFT) method accounting for dynamic electron correlation is a single-reference method, which results in the inability to describe potential energy surfaces (PESs) away from the

Received: September 26, 2023
Revised: November 10, 2023
Accepted: November 16, 2023
Published: December 6, 2023

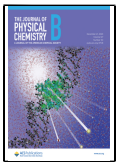

https://doi.org/10.1021/acs.jpcb.3c06433
J. Phys. Chem. B 2023, 127, 10871−10879

Franck−Condon (FC) region and in the vicinity of conical intersections (CoIns).[57] These facts make the study of the nonradiative decay channels of uracil nontrivial. The multistate multireference rotated multistate complete active space second-order perturbation (RMS-CASPT2) method offers a balanced description of PESs in both the FC and CoIn regions and it is the least sensitive to the number of states included in calculations among all variants of CASPT2 (see Lindh and co-workers)[55] Thus, in the present paper, we employ RMS-CASPT2 and quantum-classical trajectories to simulate the uracil light-induced nonadiabatic molecular dynamics (NAMD) in the gas phase and, by using suitable hybrid quantum mechanics/molecular mechanics (QM/MM) models, in a protic and an aprotic solvent.

Previous computational works on isolated (i.e., gas phase) uracil predict a lowest energy singlet excited state (S_1) with $n\pi^*$ character irrespective of the method used.[7,20,23,50−52] These results also show that the $n \rightarrow \pi^*$ transition mainly arises from the excitation of the lone pairs of the C4−O8 carbonyl group to a π^* orbital. The $\pi \rightarrow \pi^*$ transition, where an electron is promoted from the bonding to the antibonding orbital of the C5−C6 double bond, is higher in energy.[7,19,21] The orbitals involved in these excited states are shown in Figure 1. The same calculations also indicate that the $n \rightarrow \pi^*$ transition has low oscillator strength (dark state), while the $\pi \rightarrow \pi^*$ transition, featuring a much higher oscillator strength (bright state), gets populated after UV irradiation. Such energy ordering and oscillator strengths point to a mechanism involving de-excitation from $\pi\pi^*$ to $n\pi^*$ with subsequent de-excitation from $n\pi^*$ to the ground state (here indicated as S_0 or GS).[7,21,54]

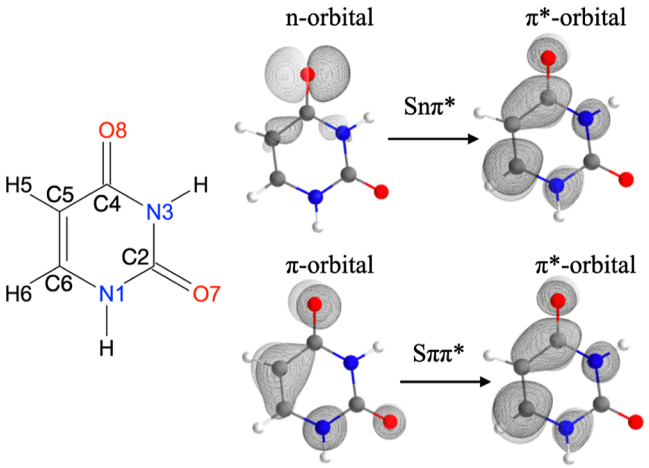

Figure 1. Singlet electronic excited states ($n\pi^*$ and $\pi\pi^*$) in uracil derived via a $n \rightarrow \pi^*$ and $\pi \rightarrow \pi^*$ transition, respectively.

In water, the situation is different, with an $n\pi^*$ state destabilized by ∼0.7 eV with respect to the $\pi\pi^*$ state. This destabilization appears to be present in any hydrogen bonding (protic) solvent.[7,40,48,58] It is also important to note that the $n\pi^*$ destabilization is actually the result of a combined ∼0.5 eV $n\pi^*$ increase and ∼0.2 eV $\pi\pi^*$ decrease in energy.[7,40,48,56] In fact, since in the $n \rightarrow \pi^*$ transition, an electron is transferred from a tight oxygen lone pair to a more diffused π^* molecular orbital, the hydrogen bonding between a water molecule and the carbonyl oxygen in $n\pi^*$ modulates the transition energy.[7,40,47] As a consequence, a model describing explicitly the interaction between uracil and its first solvation shell appears to be mandatory.[27,32,33,36,37,39,46−48,56] On the other hand, the solvent bulk also appears to play a role. For example, a recent study by Milovanović et al.[45] utilized an implicit and an explicit solvated uracil model excluding the bulk. The explicit model, corresponding to the $U(H_2O)_6$ cluster, yields a lower $n\pi^*$ state, while the implicit model indicated a lower energy $\pi\pi^*$ state. Other studies, utilizing a combination of the first solvation shell and implicit bulk, yielded a $\pi\pi^*$ stabilization.[27,32,33,36,37,39,46−48,56] The higher stability of the $\pi\pi^*$ state in water is also supported by a model describing the solvent bulk effect explicitly (see Olsen et al.[48]).

The results above suggest that the $\pi\pi^*$ state stabilization for uracil in water leads to a radiationless transition mechanism different from the one operating in the gas phase or, presumably, solvents that do not form hydrogen bonds (e.g., the aprotic solvent acetonitrile).[28,31−33,38,42,43,58] The CASSCF-based NAMD study by Nachtigallová et al.[19] as well as the combined experimental and theoretical (again with CASSCF-based NAMD) studies by Hudock et al.[50] and Fingerhut et al.[59] indicate that in the gas phase, the decay from the $\pi\pi^*$ state to S_0 occurs through both direct and indirect decay channels. A study by Chakraborty et al.[23], employing the NAMD simulations with the more advanced (similar to RMS-CASPT2) extended multistate CASPT2 (XMS-CASPT2) method that accounts for both static and dynamic electron correlation, also confirms the presence of both direct and indirect decay channels for uracil in the gas phase.

The nature of radiationless transition of uracil in acetonitrile is substantially less studied and was explored primarily with the TDDFT method lacking static electron correlation.[38,42,43] In 2006, Santoro et al.[38] elucidated the presence of direct and indirect decay channels for uracil in acetonitrile using potential energy scans calculated with a combination of TDDFT and CASSCF methods, where the CASSCF method was used for determining the conical intersection geometries. The mechanism of radiationless transition of uracil in acetonitrile was further elucidated using TDDFT-based molecular dynamics studies by Improta et al.[42] and Santoro et al.,[43] where the molecular dynamics simulations were performed on precomputed three-dimensional PESs where only three suitable coordinates were considered. Moreover, as mentioned in both studies,[42,43] while TDDFT can accurately describe the FC region, it has substantial issues when attempting to describe a CoIn region possibly making the derived deactivation mechanism uncertain.[57]

The currently proposed mechanistic hypothesis is based on the fact that the S_1 PES incorporates regions dominated by either the $\pi\pi^*$ or $n\pi^*$ electronic characters. A first hypothesis states that for uracil in the gas phase and acetonitrile, the direct decay channel from the spectroscopic $\pi\pi^*$ state to S_0 goes through a path intercepting a $\pi\pi^*/n\pi^*$ (S_2/S_1) seam but conserving the $\pi\pi^*$ character (i.e., as in a diabatic-type of transition) until the lowest $\pi\pi^*/\pi^2$ (S_1/S_0) seam delivers the system to the GS (π^2 refers to the usual closed-shell electronic structure of the S_0 or GS state). The indirect decay channel instead involves trapping of the population in the dark $n\pi^*$ state after a $\pi\pi^*/n\pi^*$ seam is reached,[7] before regenerating the $\pi\pi^*$ state during a recrossing of the same seam and, ultimately, reaching the $\pi\pi^*/\pi^2$ seam providing access to S_0. The mechanism involving direct and indirect decay channels[7] is schematically represented in the left panel of Figure 2. The above-mentioned TDDFT study by Santoro and co-workers[38]

https://doi.org/10.1021/acs.jpcb.3c06433
J. Phys. Chem. B 2023, 127, 10871−10879

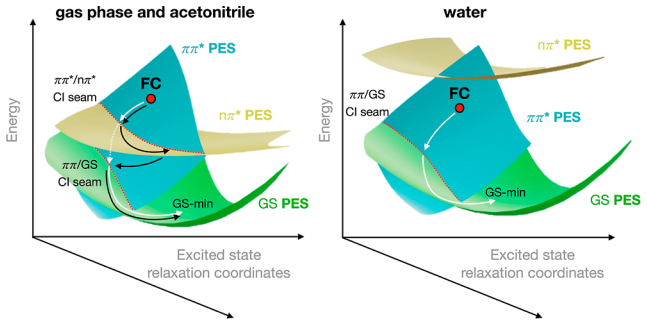

Figure 2. Qualitative picture of the singlet electronic excited state ordering and light-triggered deactivation mechanism of uracil occurring in the gas phase, acetonitrile, and water. Cyan, yellow, and green surfaces represent PESs of $\pi\pi^*$, $n\pi^*$, and the GS, respectively. The red circle symbolizes the FC point residing on the PESs of the bright $\pi\pi^*$ state. The red dashed lines represent the seam defined by the CoIns between the PESs of $\pi\pi^*$ and $n\pi^*$ and between $\pi\pi^*$ and π^2, respectively. Black arrows demonstrate the indirect decay channel, while white arrows indicate the channel not involving trapping of the population on the $n\pi^*$ PES (direct channel in acetonitrile and the gas phase as well as in water).

of the PESs of uracil in water suggested that due to the more stable $\pi\pi^*$, only a direct decay channel involving a single $\pi\pi^*/\pi^2$ (S_1/S_0) seam drives the radiationless transition of uracil (see right panel of Figure 2).

All reported NAMD simulations of uracil in water have substantial limitations.[42−45] The mentioned simulations by Santoro, Improta, and co-workers were performed (both for uracil in acetonitrile and uracil in water) on precomputed three-dimensional PESs obtained using the TDDFT method,[42,43] therefore raising substantial accuracy issues in the description of the S_1/S_0 CoIn region.[57] A different study by Nieber and Doltsinis utilized the restricted open-shell Kohn−Sham (ROKS) method.[44] ROKS can only describe the lowest excited singlet electronic state and hence has limitations in terms of the description of interactions between the S_1 and S_2 states.[60,61] Finally, the study by Milovanović et al. utilized the SCS-ADC(2) method and the $U(H_2O)_6$ cluster model containing only six explicit water molecules and, thus, did not account for the effect of the solvent bulk.[45] These limitations cast doubt on the proposed mechanisms of uracil nonradiative decay that, therefore, remain inconclusive.

In order to achieve a conclusive mechanistic understanding of the uracil photodynamics, the present study utilizes the RMS-CASPT2 method accounting for both static and dynamic electron correlation and has shown to describe CoIn regions correctly as well as QM/MM models explicitly incorporating an extended solvent region to better account for the effect of the bulk.[55] The main geometrical coordinates promoting the UV-induced nonradiative decay in uracil are the torsion angle α defined through the positions of atoms C4−C5−C6−N1, torsion angle β formed by atoms H5−C5−C6−H6, and the skeletal bond length alternation (BLA) along the conjugated part of the uracil.[23,25] These coordinates allow the description of the propagation of uracil from the FC region to the CoIn region known as "ethylenic" in the literature.[23,62] Torsion angle α, torsion angle β, and BLA are illustrated in Figure 3. Our study is based on the propagation of the entire set of the solvated uracil coordinates incorporating the chromophore and the first solvation shell, thus avoiding issues related to a restricted dimensionality of the considered PESs.

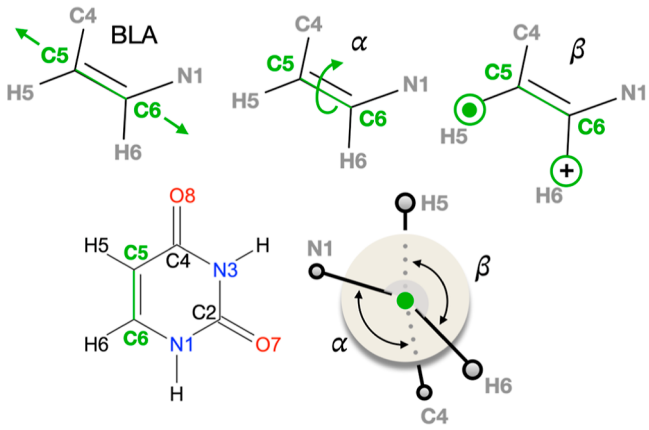

Figure 3. Reaction coordinates along the nonradiative decay pathway in uracil.

Previous studies indicated the potential importance of a ring-opening path as well as singlet/triplet transitions for photochemistry of uracil in the gas phase.[19,20,23] The role of these pathways is yet to be elucidated and will not be pursued in the present study. It is important to note that experimental work on the relaxation of excited electronic states of pyrimidine bases in water solution by Hare et al.[41] showed that the radiationless decay of uracil in water not only occurs via a fast decay (i.e., within 2 ps) but also identifies a second slower decay channel associated with an excited state lifetime of ca. 24 ps. In the present study, we only focus on the fast decay channel. Moreover, our focus is the elucidation of the qualitative (i.e., mechanistic) role of $\pi\pi^*$ and $n\pi^*$ states in controlling the fast decay channel of uracil in different solvent environments, while the quantitative description, requiring longer simulation times and larger numbers of trajectories, of the population decay for each state is outside of the scope of the present study.

COMPUTATIONAL METHODS

All calculations were performed with the 6-31G* basis set. OpenMolcas and OpenMolcas/Tinker[63−65] were used for QM and QM/MM calculations, respectively. CASSCF and RMS-CASPT2 calculations were performed as the state average over three states (GS, $Sn\pi^*$, and $S\pi\pi^*$). Our research included four types of calculations:

1. RMS-CASPT2(12,9)/6-31G*-based simulations of the absorption spectrum in the gas phase (as a reference), explicit water, and acetonitrile (in the two solvated models, uracil corresponds to the QM subsystem).
2. Gas-phase quantum-classical trajectory propagation at the RMS-CASPT2(12,9)/6-31G* and CASSCF(12,9)/6-31G* QM levels and comparison to previous studies (e.g., to the gas-phase XMS-CASPT2(12,9)/6-31G* study by Chakraborty et al.[23]).
3. Quantum-classical trajectory propagation in water and acetonitrile by using RMS-CASPT2(12,9)/6-31G*- and CASSCF(12,9)/6-31G*-based QM/MM models.
4. Minimum energy conical intersection (MECI) search at the RMS-CASPT2(12,9)/6-31G* and CASSCF(12,9)/6-31G* levels to assign the decay channels detected via trajectory analysis to specific CoIns.

Points 1 and 2 represent studies aimed at showing if RMS-CASPT2(12,9)/6-31G* is consistent with the results of

https://doi.org/10.1021/acs.jpcb.3c06433
J. Phys. Chem. B 2023, 127, 10871−10879

previous studies, while points 3 and 4 provide novel information on the dynamics of uracil in different solvent environments. More specifically, the results of point 3 are expected to demonstrate the importance of dynamic electron correlation in the simulations of uracil radiationless decay in solution. The light-induced dynamics is simulated by sets of trajectories initiated by using 365−392 initial conditions. The Supporting Information contains the structure and construction of the QM/MM model (Section 1 of Supporting Information); selected active space CAS(12,9) (Figure S2 and Section 2 of Supporting Information); details of the absorption spectrum simulations (Section 3 of Supporting Information); details of NAMD simulations with Tully's surface hopping algorithm (Section 4 of Supporting Information); and details of MECI optimizations (Section 5 of Supporting Information).

RESULTS AND DISCUSSION

Absorption Spectra. The simulated SA3-RMS-CASPT2-(12,9)/6-31G* absorption band of uracil in the gas phase showed a blue shift with respect to experimental data (Figure S3 and Section 6 of Supporting Information), while in both water and uracil, we observed a red shift (Figure 4) with

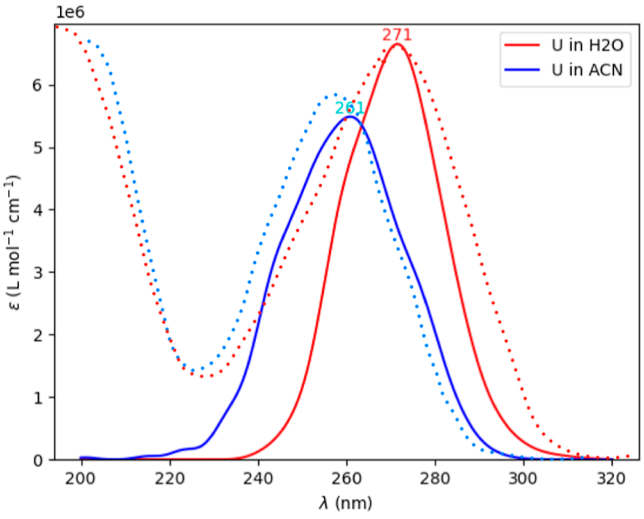

Figure 4. Comparison of simulated absorption spectra (solid lines) of uracil in water and acetonitrile with the experimental spectra (dotted lines). The experimental data for uracil in water and acetonitrile are from refs 40 and 29, respectively.

deviations of 11 and 5 nm for water and acetonitrile, respectively. Table 1 shows the maxima of the simulated and experimental absorption bands as well as the vertical excitation energies (VEEs) of S$\pi\pi^*$ and Snπ^* calculated at the ground-state minimum geometries of each system.

Table 1. Absorption Band Maxima (λ_{max}) of Uracil in Water and Acetonitrile Calculated with the RMS-CASPT2 Method Compared with the Experimental Values (refs 29 and 40) and VEEs to S$\pi\pi^*$ Calculated for Each Solvent at the Geometries of the GS Minimum

solvent	calculated λ_{max}, nm (eV)	experimental λ_{max}, nm (eV)	S$\pi\pi^*$ VEE, eV	Snπ^* VEE, eV
water	271 (4.58)	260 (4.77)[a]	4.95	5.44
acetonitrile	261 (4.75)	256 (4.84)[b]	4.99	4.89

[a]Reference 40. [b]Reference 29.

In uracil, the computed bright $\pi \rightarrow \pi^*$ transition in acetonitrile shows a λ_{max} slightly blue-shifted with respect to water: a prediction consistent with previous theoretical works and with experimental observations.[29,38,40,42,43] The shift is the result of the stabilization of the $\pi\pi^*$ state induced by formation of hydrogen bonds between the solute and the solvent as well as by the polarization by the solvent bulk. This effect together with the destabilization of the nπ^* state induced by the same factors was reported in previous studies.[27,28,31−33,36−39,42,43,46−48,56,58]

Population Dynamics of Uracil. We first compare the qualitative agreement of our SA3-RMS-CASPT2(12,9)/6-31G* and SA3-CASSCF(12,9)/6-31G* quantum-classical trajectories in the gas phase with previously published XMS-CASPT2 and CASSCF gas-phase simulations by Chakraborty et al.[23] Specifically, we compare the behavior of our trajectories (Figure S4), the resulting surface hopping points (Figure S5), and the MECI structures located starting from specific clusters of hopping points. We show the results of uracil gas-phase simulations in Section 7 of the Supporting Information. Briefly, we observe that the distribution of surface hopping points in our calculations is in qualitative agreement with the results of CASSCF and XMS-CASPT2 NAMD simulations by Chakraborty et al.[23] The CASSCF and XMS-CASPT2 MECI structures predicted in our work deviate by <1° in value of torsion angle β and by <0.2 Å in bond lengths of C6 = C5 and C4 = O8 bonds from the structures predicted by Chakraborty et al.[23]

Dynamics in Water. Consistent with previous studies,[32,37,48] the RMS-CASPT2 level predicts the $\pi\pi^*$ state of uracil in water to be substantially stabilized with respect to the nπ^* state due to dynamic electron correlation effects. In contrast, our CASSCF calculations confirm that such a level of theory does not correctly describe the $\pi\pi^*$ state stability that is found to be higher than the nπ^* state (i.e., at the CASSCF level, the $\pi\pi^*$ state of uracil in water is S_2).[32,37,48] These differences lead to different CASSCF- and RMS-CASPT2-driven dynamics. CASSCF trajectories feature $\pi\pi^*/n\pi^*$, $n\pi^*/\pi\pi^*$, and $\pi\pi^*/\pi^2$ transitions with $\pi\pi^*/n\pi^*$ hops already occurring during the first 10 fs (Figure 5A,C,E). However, the majority of $\pi\pi^*/n\pi^*$ transitions occur between 50 and 200 fs, while the following $n\pi^*/\pi\pi^*$ and $\pi\pi^*/\pi^2$ surface hops are distributed along 200 fs with a higher density of surface hopping points in the first 100 fs. In contrast with CASSCF, RMS-CASPT2 trajectories in water do not produce $\pi\pi^*/\pi^2$ transitions before 50 fs of progression but display an even distribution of $\pi\pi^*/\pi^2$ hopping points from 50 to 200 fs (Figure 5B,D,F). Notably, the percentage of trajectories that decayed to S_0 in 200 fs of CASSCF simulations is 50%, which is higher than the 25% observed in 200 fs of RMS-CASPT2 simulations.

Figure 6 displays the geometrical distribution of surface hopping points predicted by the CASSCF and RMS-CASPT2 trajectories in terms of α and β torsions. The CASSCF search for the MECI starting from independent groups of hopping points reveals the presence of $\pi\pi^*/n\pi^*$, $n\pi^*/\pi\pi^*$, and $\pi\pi^*/\pi^2$ MECIs. The RMS-CASPT2 search for the MECI initiated from $\pi\pi^*/\pi^2$ hopping points predicted by RMS-CASPT2 NAMD allowed us to locate the $\pi\pi^*/\pi^2$ MECI.

The CASSCF calculations produce the $\pi\pi^*/n\pi^*$ MECI with β = 53°, $n\pi^*/\pi\pi^*$ MECI with β = 21°, and the $\pi\pi^*/\pi^2$ MECI

https://doi.org/10.1021/acs.jpcb.3c06433
J. Phys. Chem. B 2023, 127, 10871−10879

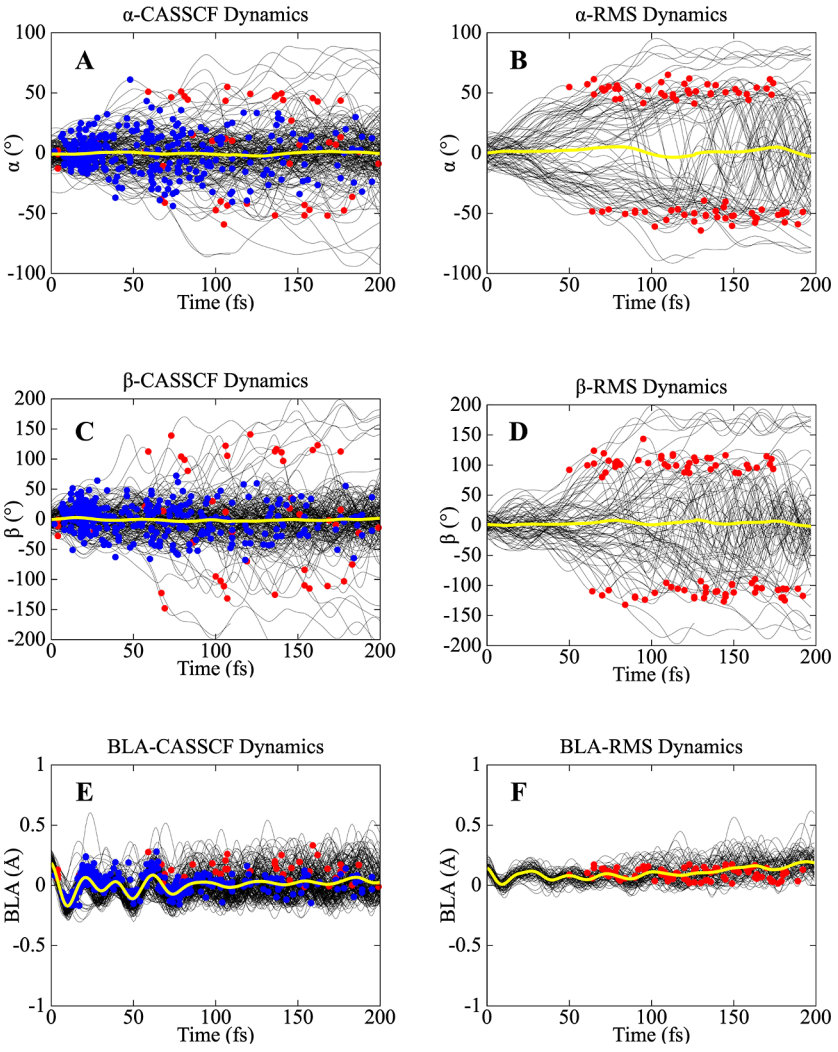

Figure 5. Evolution of the torsion angle α (panels A,B), torsion angle β (panels C,D), and BLA (panels E,F) described by NAMD of uracil in water. The CASSCF results are presented in panels A, C, and E, while the RMS-CASPT2 (marked as "RMS") results are presented in panels B, D, and F. The solid black lines represent propagation of individual trajectories along the given coordinate. The blue dots represent the transitions leading to trapping of the population on the nπ^* PES ($\pi\pi^*/n\pi^*$ transitions), while the red points represent surface hops promoting decay toward the GS ($n\pi^*/\pi\pi^*$ and $\pi\pi^*/\pi^2$ transitions).

with $\beta = 118°$. These MECIs define a mechanism involving the direct and indirect decay channels similar to what is observed in the gas phase (see Supporting Information). The presence of these MECIs indicates that CASSCF predicts the same mixed mechanism in water and the gas phase. This involves direct and indirect decay channels as summarized in the review by Improta et al.[7] and shown in Figure 2 above. However, previous works by Improta et al.,[40] Santoro et al.,[38] as well as simulations by Nieber and Doltsinis[44] show that the inclusion of dynamic electron correlation (lacking in CASSCF) does not support a mixed mechanism in water. Our RMS-CASPT2 NAMD and MECI simulations, incorporating both static and dynamic electron correlation, conclusively demonstrate that this is indeed the case for uracil in water as the decay to the closed-shell GS only involves $\pi\pi^*/\pi^2$ transition (see Figures 5 and 6). We argue that the QM/MM-driven simulations based on RMS-CASPT2 are ideal tools for uracil photochemistry studies in water. Note that the experimental work by Hare et al.[41] not only shows the presence of fast decay channels occurring within 2 ps but also identifies the presence of a channel associated with an excited state lifetime of 24 ± 2 ps. This second channel is not investigated in the present work and requires future studies with substantially longer simulation time.

Dynamics in Acetonitrile. In contrast to the water environment, the CASSCF- and RMS-CASPT2-driven NAMD of uracil in acetonitrile predict a similar mechanism involving direct and indirect decay channels resembling gas-phase uracil. For this reason, here we focus exclusively on RMS-CASPT2 simulations, while CASSCF simulations are described in Section 8 of the Supporting Information (see also Figures S6 and S7). RMS-CASPT2 trajectories display, consistently with the gas-phase simulations, $\pi\pi^*/n\pi^*$, $n\pi^*/\pi\pi^*$, and $\pi\pi^*/\pi^2$ transitions during the first 10 fs of simulations (Figure 7A−C). Another similarity between the behavior of uracil in the gas phase and uracil in acetonitrile is the predominance of $n\pi^*/\pi\pi^*$ and $\pi\pi^*/\pi^2$ transitions between 50 and 200 fs. However, in contrast to the gas phase, where $\pi\pi^*/n\pi^*$ transitions predominantly occur within the first 50 fs, in acetonitrile, we see an even distribution of these decay points along the entire 200 fs RMS-CASPT2 simulation. At the end of the simulation, we observe 21% of trajectories reaching S_0.

https://doi.org/10.1021/acs.jpcb.3c06433
J. Phys. Chem. B 2023, 127, 10871−10879

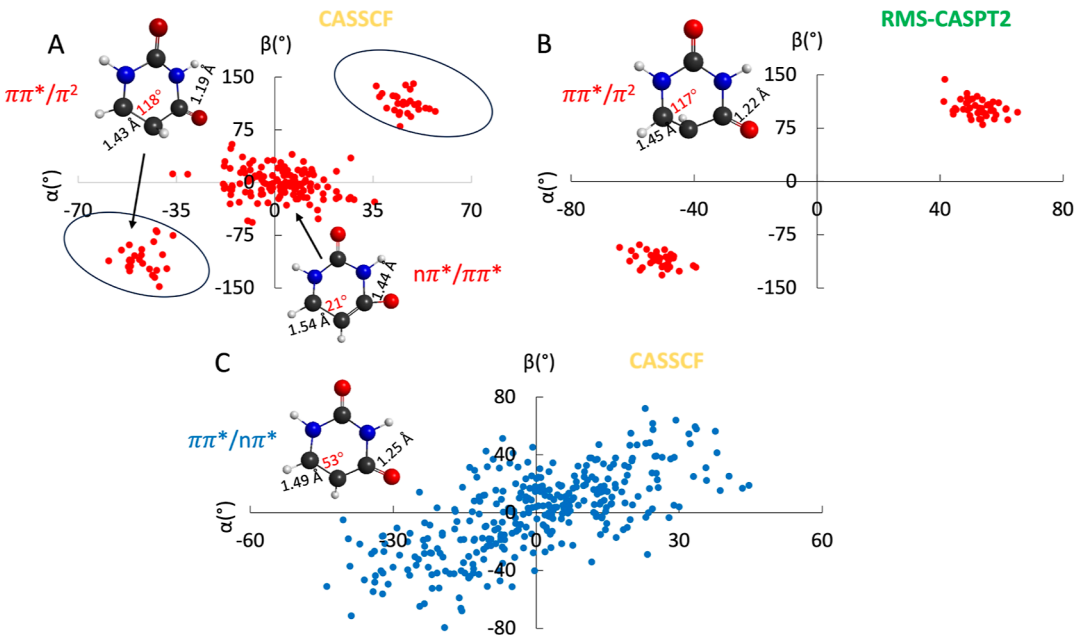

Figure 6. Distribution of surface hopping points in CASSCF and RMS-CASPT2 NAMD simulations of uracil in water as a function of torsion angles α and β. (A) CASSCF n$\pi^*/\pi\pi^*$ and $\pi\pi^*/\pi^2$ surface hopping points. (B) RMS-CASPT2 $\pi\pi^*/\pi^2$ surface hopping points. (C) CASSCF $\pi\pi^*/$nπ^* surface hopping points. The blue dots represent the transitions leading to trapping of the population on the nπ^* PES ($\pi\pi^*/$nπ^* transitions), while the red points represent surface hops promoting decay toward the GS (n$\pi^*/\pi\pi^*$ and $\pi\pi^*/\pi^2$ transitions). Inserts demonstrate MECI geometries that are located by initiating MECI search from surface hopping points of a given group of trajectories.

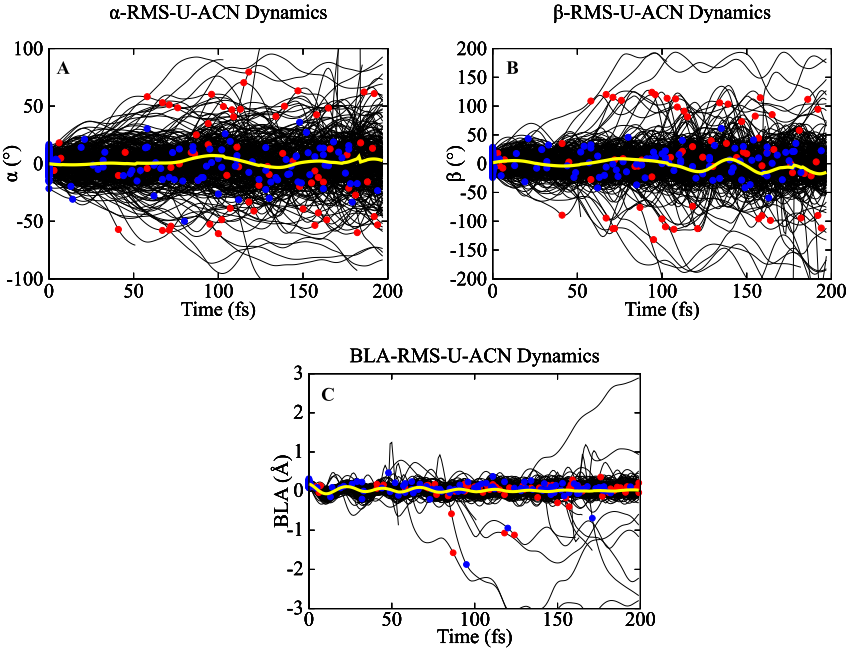

Figure 7. Propagation of the torsion angle α (panel A), torsion angle β (panel B), and BLA (panel C) along the RMS-CASPT2 trajectories of uracil in acetonitrile. The solid black lines represent propagation of individual trajectories along the given coordinate. The blue dots represent the transitions ($\pi\pi^*/$nπ^*) leading to trapping of the population on an nπ^*-dominated region of the S_1 PES, while the red points represent surface hops promoting decay toward the GS (n$\pi^*/\pi\pi^*$ and $\pi\pi^*/\pi^2$ transitions).

In Figure 8, we report the distribution of $\pi\pi^*/$nπ^*, n$\pi^*/\pi\pi^*$, and $\pi\pi^*/\pi^2$ surface hopping points predicted with RMS-CASPT2 simulations in terms of the torsion angles α and β. By performing MECI calculations, starting with representatives of the diverse clusters of hopping points, we identify the geometries of the $\pi\pi^*/$nπ^*, n$\pi^*/\pi\pi^*$, and $\pi\pi^*/\pi^2$ MECIs. The results of the corresponding CASSCF-driven simulations are discussed in the Supporting Information and summarized in Figures S6 and S7.

The RMS-CASPT2 calculations of uracil in acetonitrile produce the $\pi\pi^*/$nπ^* MECI with $\beta = 8°$, n$\pi^*/\pi\pi^*$ MECI with $\beta = 29°$, and $\pi\pi^*/\pi^2$ MECI with $\beta = 115°$. As can be seen in Figures 8 and S7, both RMS-CASPT2 and CASSCF simulations predict mechanisms involving direct and indirect decay channels. However, there is a quantitative difference in

https://doi.org/10.1021/acs.jpcb.3c06433
J. Phys. Chem. B 2023, 127, 10871−10879

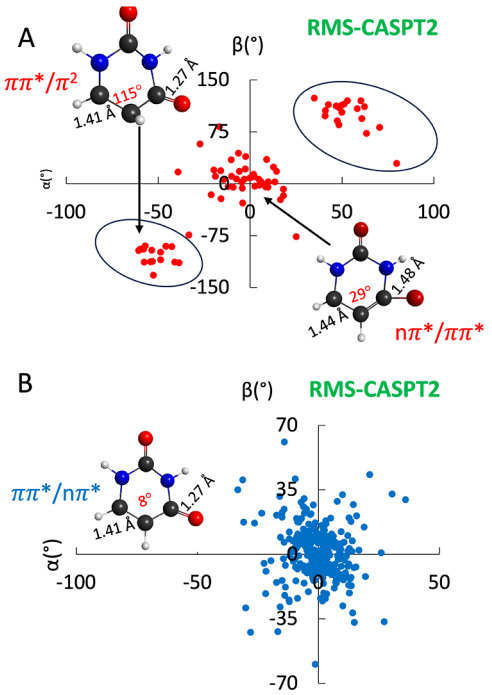

Figure 8. Distribution of surface hopping points in RMS-CASPT2 NAMD simulations of uracil in acetonitrile as a function of torsion angles α and β. (A) RMS-CASPT2 n$\pi^*/\pi\pi^*$ and $\pi\pi^*/\pi^2$ surface hopping points. (B) RMS-CASPT2 $\pi\pi^*$/nπ^* surface hopping points. The blue dots represent the transitions leading to trapping of the population on the nπ^* PES ($\pi\pi^*$/nπ^* transitions), while the red points represent surface hops promoting decay toward the GS (nπ^*/$\pi\pi^*$ and $\pi\pi^*/\pi^2$ transitions). Inserts demonstrate MECI geometries that are located by initiating MECI search from surface hopping points of a given group of trajectories.

their predictions in terms of the width of the $\pi\pi^*$/nπ^* decay channel. CASSCF-based simulations predict $\pi\pi^*$/nπ^* hopping points distributed between α values in the 0−50° range and β values in the 0−100° range, while the RMS-CASPT2 simulations show that the majority of $\pi\pi^*$/nπ^* hopping points have α values in the 0−20° range and β values in the 0−35° range. Importantly, the CASSCF MECI search for the $\pi\pi^*$/nπ^* channel predicted the MECI geometry with the value of β equal to 58°, while the RMS-CASPT2MECI search identified the $\pi\pi^*$/nπ^* MECI with the β value equal to only 8°. Hence, even though CASSCF simulations predict a broader $\pi\pi^*$/nπ^* channel with respect to RMS-CASPT2 simulations, the CASSCF method predicts the MECI to be located farther away from the FC than RMS-CASPT2.

CONCLUSIONS

By using QM/MM RMS-CASPT2 NAMD and MECI calculations with explicit solvent, it is possible to investigate the radiationless deactivation of the $\pi\pi^*$ state of uracil in different environments taking into account the effects of both dynamic and nondynamic electron correlation as well as, partially, of the solvent bulk. It is found that the excited state decay to the closed-shell GS in the gas phase and acetonitrile involves three electronic states and both the direct and indirect decay channels, illustrated in Figure 2. It is confirmed that the direct decay channel from the $\pi\pi^*$ state goes through the $\pi\pi^*$/nπ^* seam without changing the initial $\pi\pi^*$ character, while the indirect decay channel involves trapping of the population in the dark nπ^* state. We show that, in spite of the general similarities mentioned above, for uracil in acetonitrile where one detects both direct and indirect decay channels, the RMS-CASPT2-based simulations predict a $\pi\pi^*$/nπ^* channel narrower than the one obtained using CASSCF.

The existence of separate mechanisms for the gas phase and acetonitrile environments vs the water environment is not seen in CASSCF-based simulations, indicating the pivotal and possibly dominating role of dynamic electron correlation for the modelization of the photoresponse of nucleobases. Indeed, the investigated RMS-CASPT2 level of theory confirms the reported TDDFT and ROKS results, also accounting for dynamic electron correlation. In conclusion, we have provided evidence supporting the use of RMS-CASPT2-based simulations for a balanced study of uracil photodynamics both in the gas phase and in qualitatively different solvent environments.

ASSOCIATED CONTENT

Supporting Information

The Supporting Information is available free of charge at https://pubs.acs.org/doi/10.1021/acs.jpcb.3c06433.

Uracil QM and QM/MM model construction, selection of active space; details of absorption spectra, details of NAMD simulations with Tully's surface hopping algorithm, details of MECI calculations, results of gas-phase absorption spectrum simulations, results of uracil in gas-phase NAMD simulations, and results of uracil in acetonitrile CASSCF NAMD simulations (PDF)

AUTHOR INFORMATION

Corresponding Authors

Danil S. Kaliakin − *Department of Chemistry, Bowling Green State University, Bowling Green, Ohio 43403, United States;* orcid.org/0000-0002-9354-8248; Email: dskalyakin@outlook.com

Massimo Olivucci − *Department of Chemistry, Bowling Green State University, Bowling Green, Ohio 43403, United States; Dipartimento di Biotechnologie, Chimica e Farmacia, Università di Siena, I-53100 Siena, Italy;* orcid.org/0000-0002-8247-209X; Email: olivucci@unisi.it, molivuc@bgsu.edu

Authors

Meseret Simachew Bezabih − *Department of Chemistry, Bowling Green State University, Bowling Green, Ohio 43403, United States*

Alejandro Blanco-González − *Department of Chemistry, Bowling Green State University, Bowling Green, Ohio 43403, United States;* orcid.org/0000-0001-7379-2588

Leonardo Barneschi − *Dipartimento di Biotechnologie, Chimica e Farmacia, Università di Siena, I-53100 Siena, Italy*

Alexander N. Tarnovsky − *Department of Chemistry, Bowling Green State University, Bowling Green, Ohio 43403, United States;* orcid.org/0000-0001-7918-2676

Complete contact information is available at: https://pubs.acs.org/10.1021/acs.jpcb.3c06433

Notes

The authors declare no competing financial interest.

https://doi.org/10.1021/acs.jpcb.3c06433
J. Phys. Chem. B 2023, 127, 10871−10879

■ ACKNOWLEDGMENTS

A.N.T., M.O., and D.S.K. acknowledge support from NSF CSDM-A grant no. 2102619. M.O. is also grateful for European-Union, Next Generation EU, MIUR Italia Domani Progetto mRNA Spoke 6 del "National Center for Gene Therapy and Drugs based on RNA Technology". C.U.P. B63C22000610006. M.S.B. expresses gratitude to Laura M. Obloy for a detailed discussion regarding experimental data on uracil photophysics and photochemistry previously established in the literature.

■ DEDICATION

This article has been written in honor of Prof. Roland Lindh for his 65th birthday and of Prof. Maurizio Persico for his retirement.

■ REFERENCES

(1) Douki, T. The Variety of UV-Induced Pyrimidine Dimeric Photoproducts in DNA as Shown by Chromatographic Quantification Methods. *Photochem. Photobiol. Sci.* **2013**, *12*, 1286−1302.
(2) *Bioorganic Photochemistry. Photochemistry and the Nucleic Acids*; Morrison, H., Ed.; Wiley-Interscience: New York, 1990; Vol. *1*.
(3) Taylor, J. S. Unraveling the Molecular Pathway from Sunlight to Skin Cancer. *Acc. Chem. Res.* **1994**, *27*, 76−82.
(4) Batista, L. F. Z.; Kaina, B.; Meneghini, R.; Menck, C. F. M. How DNA Lesions Are Turned into Powerful Killing Structures: Insights from UV-Induced Apoptosis. *Mutat. Res., Rev. Mutat. Res.* **2009**, *681*, 197−208.
(5) Melnikova, V. O.; Ananthaswamy, H. N. Cellular and Molecular Events Leading to the Development of Skin Cancer. *Mutat. Res., Fundam. Mol. Mech. Mutagen.* **2005**, *571*, 91−106.
(6) Sage, E.; Girard, P. M.; Francesconi, S. Unravelling UVA-Induced Mutagenesis. *Photochem. Photobiol. Sci.* **2012**, *11*, 74−80.
(7) Improta, R.; Santoro, F.; Blancafort, L. Quantum Mechanical Studies on the Photophysics and the Photochemistry of Nucleic Acids and Nucleobases. *Chem. Rev.* **2016**, *116*, 3540−3593.
(8) Bonella, S.; Coker, D. F.; Kapral, R.; Ciccotti, G. *Energy Transfer Dynamics in Biomaterial Systems*; Springer, 2009; Vol. *93*, pp 103−165.
(9) Kwon, Y. W.; Lee, C. H.; Choi, D. H.; Jin, J. Il. Materials Science of DNA. *J. Mater. Chem.* **2009**, *19*, 1353−1380.
(10) Gomez, E. F.; Venkatraman, V.; Grote, J. G.; Steckl, A. J. Organic Light-Emitting Diodes: Exploring the Potential of Nucleic Acid Bases in Organic Light Emitting Diodes (Adv. Mater. 46/2015). *Adv. Mater.* **2015**, *27*, 7680.
(11) *Radiation Induced Molecular Phenomena in Nucleic Acids*; Manoj, K., Shukla, J. L., Eds.; Springer Science, 2008.
(12) Crespo-Hernandez, C. E.; Cohen, B.; Hare, P. M.; Kohler, B. Ultrafast Excited-State Dynamics in Nucleic Acids. *Chem. Rev.* **2004**, *104*, 1977−2020.
(13) Middleton, C. T.; De La Harpe, K.; Su, C.; Law, Y. K.; Crespo-Hernández, C. E.; Kohler, B. DNA Excited-State Dynamics: From Single Bases to the Double Helix. *Annu. Rev. Phys. Chem.* **2009**, *60*, 217−239.
(14) Schreier, W. J.; Gilch, P.; Zinth, W. Early Events of DNA Photodamage. *Annu. Rev. Phys. Chem.* **2015**, *66*, 497−519.
(15) Gengeliczki, Z.; Callahan, M. P.; Svadlenak, N.; Pongor, C. I.; Sztáray, B.; Meerts, L.; Nachtigallová, D.; Hobza, P.; Barbatti, M.; Lischka, H.; et al. Effect of Substituents on the Excited-State Dynamics of the Modified DNA Bases 2,4-Diaminopyrimidine and 2,6-Diaminopurine. *Phys. Chem. Chem. Phys.* **2010**, *12*, 5375−5388.
(16) Barbatti, M.; Borin, A. C.; Ullrich, S. *Photoinduced Phenomena in Nucleic Acids I. Nucleobases in the Gas Phase and in Solvents*; Springer, 2015; Vol. *355*, pp 1−329.
(17) Barbatti, M.; Ullrich, S.; Borin, A. C. *Photoinduced Phenomena in Nucleic Acids II DNA Fragments and Phenomenological Aspects*; Springer, 2015; Vol. *356*, pp 1−249.
(18) Yu, H.; Sanchez-Rodriguez, J. A.; Pollum, M.; Crespo-Hernández, C. E.; Mai, S.; Marquetand, P.; González, L.; Ullrich, S. Internal Conversion and Intersystem Crossing Pathways in UV Excited, Isolated Uracils and Their Implications in Prebiotic Chemistry. *Phys. Chem. Chem. Phys.* **2016**, *18*, 20168−20176.
(19) Nachtigallová, D.; Aquino, A. J. A.; Szymczak, J. J.; Barbatti, M.; Hobza, P.; Lischka, H. Nonadiabatic Dynamics of Uracil: Population Split among Different Decay Mechanisms. *J. Phys. Chem. A* **2011**, *115*, 5247−5255.
(20) Richter, M.; Mai, S.; Marquetand, P.; González, L. Ultrafast Intersystem Crossing Dynamics in Uracil Unravelled by Ab Initio Molecular Dynamics. *Phys. Chem. Chem. Phys.* **2014**, *16*, 24423−24436.
(21) Fedotov, D. A.; Paul, A. C.; Posocco, P.; Santoro, F.; Garavelli, M.; Koch, H.; Coriani, S.; Improta, R. Excited-State Absorption of Uracil in the Gas Phase: Mapping the Main Decay Paths by Different Electronic Structure Methods. *J. Chem. Theory Comput.* **2021**, *17*, 1638−1652.
(22) Merchán, M.; González-Luque, R.; Climent, T.; Serrano-Andrés, L.; Rodríguez, E.; Reguero, M.; Peláez, D. Unified Model for the Ultrafast Decay of Pyrimidine Nucleobases. *J. Phys. Chem. B* **2006**, *110*, 26471−26476.
(23) Chakraborty, P.; Liu, Y.; Weinacht, T.; Matsika, S. Effect of Dynamic Correlation on the Ultrafast Relaxation of Uracil in the Gas Phase. *Faraday Discuss.* **2021**, *228*, 266−285.
(24) Matsika, S. Radiationless Decay of Excited States of Uracil through Conical Intersections. *J. Phys. Chem. A* **2004**, *108*, 7584−7590.
(25) Park, W.; Filatov (gulak), M.; Sadiq, S.; Gerasimov, I.; Lee, S.; Joo, T.; Choi, C. H. A Plausible Mechanism of Uracil Photohydration Involves an Unusual Intermediate. *J. Phys. Chem. Lett.* **2022**, *13*, 7072−7080.
(26) Gustavsson, T.; Sarkar, N.; Bányász, Á.; Markovitsi, D.; Improta, R. Solvent Effects on the Steady-State Absorption and Fluorescence Spectra of Uracil, Thymine and 5-Fluorouracil. *Photochem. Photobiol.* **2007**, *83*, 595−599.
(27) Cornetta, L. M.; Coutinho, K.; Varella, M. T. D. N. Solvent Effects on the Π* Shape Resonances of Uracil. *J. Chem. Phys.* **2020**, *152*, 084301.
(28) Domcke, W.; Sobolewski, A. Molecular mechanisms of the photostability of life. *Phys. Chem. Chem. Phys.* **2010**, *12*, 4897−4898.
(29) Gustavsson, T.; Sarkar, N.; Lazzarotto, E.; Markovitsi, D.; Improta, R. Singlet Excited State Dynamics of Uracil and Thymine Derivatives: A Femtosecond Fluorescence Upconversion Study in Acetonitrile. *Chem. Phys. Lett.* **2006**, *429*, 551−557.
(30) Zazza, C.; Olsen, J. M.; Kongsted, J. Solvatochromic Shifts vs Nanosolvation Patterns: Uracil in Water as a Test Case. *Comput. Theor. Chem.* **2011**, *974*, 109−116.
(31) Yoshikawa, A.; Matsika, S. Excited Electronic States and Photophysics of Uracil-Water Complexes. *Chem. Phys.* **2008**, *347*, 393−404.
(32) Bistafa, C.; Georg, H. C.; Canuto, S. Combining Ab Initio Multiconfigurational and Free Energy Gradient Methods to Study the π-π* Excited State Structure and Properties of Uracil in Water. *Comput. Theor. Chem.* **2014**, *1040−1041*, 312−320.
(33) Ludwig, V.; Coutinho, K.; Canuto, S. A Monte Carlo-Quantum Mechanics Study of the Lowest n-π* and π-π* States of Uracil in Water. *Phys. Chem. Chem. Phys.* **2007**, *9*, 4907−4912.
(34) Zazza, C.; Amadei, A.; Sanna, N.; Grandi, A.; Chillemi, G.; Di Nola, A.; D'Abramo, M.; Aschi, M. Theoretical Modeling of the Valence UV Spectra of 1,2,3-Triazine and Uracil in Solution. *Phys. Chem. Chem. Phys.* **2006**, *8*, 1385−1393.
(35) Höfener, S.; Gomes, A. S. P.; Visscher, L. Solvatochromic Shifts from Coupled-Cluster Theory Embedded in Density Functional Theory. *J. Chem. Phys.* **2013**, *139*, 104106.
(36) Mercier, Y.; Santoro, F.; Reguero, M.; Improta, R. The Decay from the Dark Nπ* Excited State in Uracil: An Integrated CASPT2/CASSCF and PCM/TD-DFT Study in the Gas Phase and in Water. *J. Phys. Chem. B* **2008**, *112*, 10769−10772.

https://doi.org/10.1021/acs.jpcb.3c06433
J. Phys. Chem. B 2023, 127, 10871−10879

(37) Defusco, A.; Ivanic, J.; Schmidt, M. W.; Gordon, M. S. Solvent-Induced Shifts in Electronic Spectra of Uracil. *J. Phys. Chem. A* **2011**, *115*, 4574−4582.
(38) Santoro, F.; Barone, V.; Gustavsson, T.; Improta, R. Solvent Effect on the Singlet Excited-State Lifetimes of Nucleic Acid Bases: A Computational Study of 5-Fluorouracil and Uracil in Acetonitrile and Water. *J. Am. Chem. Soc.* **2006**, *128*, 16312−16322.
(39) Ren, H. S.; Li, Y. K.; Zhu, Q.; Zhu, J.; Li, X. Y. Spectral Shifts of the n → π^* and π → π^* Transitions of Uracil Based on a Modified Form of Solvent Reorganization Energy. *Phys. Chem. Chem. Phys.* **2012**, *14*, 13284−13291.
(40) Gustavsson, T.; Bányász, Á.; Lazzarotto, E.; Markovitsi, D.; Scalmani, G.; Frisch, M. J.; Barone, V.; Improta, R. Singlet Excited-State Behavior of Uracil and Thymine in Aqueous Solution: A Combined Experimental and Computational Study of 11 Uracil Derivatives. *J. Am. Chem. Soc.* **2006**, *128*, 607−619.
(41) Hare, P. M.; Crespo-Hernández, C. E.; Kohler, B. Internal Conversion to the Electronic Ground State Occurs via Two Distinct Pathways for Pyrimidine Bases in Aqueous Solution. *Proc. Natl. Acad. Sci. U.S.A.* **2007**, *104*, 435−440.
(42) Improta, R.; Barone, V.; Lami, A.; Santoro, F. Quantum Dynamics of the Ultrafast $\pi\pi^*$/nπ^* Population Transfer in Uracil and 5-Fluoro-Uracil in Water and Acetonitrile. *J. Phys. Chem. B* **2009**, *113*, 14491−14503.
(43) Santoro, F.; Improta, R.; Barone, V. Three-Dimensional Diabatic Models for the $\Pi\pi^*$ → Nπ^*excited-State Decay of Uracil Derivatives in Solution. *Theor. Chem. Acc.* **2009**, *123*, 273−286.
(44) Nieber, H.; Doltsinis, N. L. Elucidating Ultrafast Nonradiative Decay of Photoexcited Uracil in Aqueous Solution by Ab Initio Molecular Dynamics. *Chem. Phys.* **2008**, *347*, 405−412.
(45) Milovanović, B.; Novak, J.; Etinski, M.; Domcke, W.; Došlić, N. Simulation of UV Absorption Spectra and Relaxation Dynamics of Uracil and Uracil-Water Clusters. *Phys. Chem. Chem. Phys.* **2021**, *23*, 2594−2604.
(46) Improta, R.; Barone, V. PCM/TD-DFT Study of the Two Lowest Excited States of Uracil Derivatives in Solution: The Effect of the Functional and of the Cavity Model. *J. Mol. Struct.: THEOCHEM* **2009**, *914*, 87−93.
(47) Bányász, Á.; Karpati, S.; Mercier, Y.; Reguero, M.; Gustavsson, T.; Markovitsi, D.; Improta, R. The Peculiar Spectral Properties of Amino-Substituted Uracils: A Combined Theoretical and Experimental Study. *J. Phys. Chem. B* **2010**, *114*, 12708−12719.
(48) Olsen, J. M.; Aidas, K.; Mikkelsen, K. V.; Kongsted, J. Solvatochromic Shifts in Uracil: A Combined MD-QM/MM Study. *J. Chem. Theory Comput.* **2010**, *6*, 249−256.
(49) Zgierski, M. Z.; Patchkovskii, S.; Fujiwara, T.; Lim, E. C. On the Origin of the Ultrafast Internal Conversion of Electronically Excited Pyrimidine Bases. *J. Phys. Chem. A* **2005**, *109*, 9384−9387.
(50) Hudock, H. R.; Levine, B. G.; Thompson, A. L.; Satzger, H.; Townsend, D.; Gador, N.; Ullrich, S.; Stolow, A.; Martínez, T. J. Ab Initio Molecular Dynamics and Time-Resolved Photoelectron Spectroscopy of Electronically Excited Uracil and Thymine. *J. Phys. Chem. A* **2007**, *111*, 8500−8508.
(51) Epifanovsky, E.; Kowalski, K.; Fan, P. D.; Valiev, M.; Matsika, S.; Krylov, A. I. On the Electronically Excited States of Uracil. *J. Phys. Chem. A* **2008**, *112*, 9983−9992.
(52) Etinski, M.; Fleig, T.; Marian, C. M. Intersystem Crossing and Characterization of Dark States in the Pyrimidine Nucleobases Uracil, Thymine, and 1-Methylthymine. *J. Phys. Chem. A* **2009**, *113*, 11809−11816.
(53) Fingerhut, B. P.; Dorfman, K. E.; Mukamel, S. Probing the Conical Intersection Dynamics of the RNA Base Uracil by UV-Pump Stimulated-Raman-Probe Signals; Ab Initio Simulations. *J. Chem. Theory Comput.* **2014**, *10*, 1172−1188.
(54) Matsika, S.; Spanner, M.; Kotur, M.; Weinacht, T. C. Ultrafast Relaxation Dynamics of Uracil Probed via Strong Field Dissociative Ionization. *J. Phys. Chem. A* **2013**, *117*, 12796−12801.
(55) Nishimoto, Y.; Battaglia, S.; Lindh, R. Analytic First-Order Derivatives of (X) MS, XDW, and RMS Variants of the CASPT2 and RASPT2Methods. *J. Chem. Theory Comput.* **2022**, *18*, 4269−4281.
(56) Kistler, K. A.; Matsika, S. Solvatochromic Shifts of Uracil and Cytosine Using a Combined Multireference Configuration Interaction/Molecular Dynamics Approach and the Fragment Molecular Orbital Method. *J. Phys. Chem. A* **2009**, *113*, 12396−12403.
(57) Levine, B. G.; Ko, C.; Quenneville, J.; MartÍnez, T. J. Conical Intersections and Double Excitations in Time-Dependent Density Functional Theory. *Mol. Phys.* **2006**, *104*, 1039−1051.
(58) Gustavsson, T.; Sarkar, N.; Lazzarotto, E.; Markovitsi, D.; Barone, V.; Improta, R. Solvent Effect on the Singlet Excited-State Dynamics of 5-Fluorouracil in Acetonitrile as Compared with Water. *J. Am. Chem. Soc.* **2006**, *110*, 12843−12847.
(59) Fingerhut, B. P.; Dorfman, K. E.; Mukamel, S. Monitoring Nonadiabatic Dynamics of the RNA Base Uracil by UV Pump-IR Probe Spectroscopy. *J. Phys. Chem. Lett.* **2013**, *4*, 1933−1942.
(60) Grimm, S.; Nonnenberg, C.; Frank, I. Restricted Open-Shell Kohn-Sham Theory for π-π^* Transitions. I. Polyenes, Cyanines, and Protonated Imines. *J. Chem. Phys.* **2003**, *119*, 11574−11584.
(61) Frank, I.; Hutter, J.; Marx, D.; Parrinello, M. Molecular Dynamics in Low-Spin Excited States. *J. Chem. Phys.* **1998**, *108*, 4060−4069.
(62) Barbatti, M.; Aquino, A. J. A.; Szymczak, J. J.; Nachtigallová, D.; Hobza, P.; Lischka, H. Relaxation Mechanisms of UV-Photoexcited DNA and RNA Nucleobases. *Proc. Natl. Acad. Sci. U.S.A.* **2010**, *107*, 21453−21458.
(63) Fdez Galván, I.; Vacher, M.; Alavi, A.; Angeli, C.; Aquilante, F.; Autschbach, J.; Bao, J. J.; Bokarev, S. I.; Bogdanov, N. A.; Carlson, R. K.; et al. OpenMolcas: From Source Code to Insight. *J. Chem. Theory Comput.* **2019**, *15*, 5925−5964.
(64) Manni, G. L.; Galván, I. F.; Alavi, A.; Aquilante, F.; Autschbach, J.; Baiardi, A.; Bao, J. J.; Battaglia, S.; Blanco-González, A.; Bokarev, S. I.; et al. The OpenMolcas Web: A Community-Driven Approach to Advancing Computational Chemistry. *J. Chem. Theory Comput.* **2023**, *19*, 6933.
(65) Ponder, J. W.; Richards, F. M. An Efficient Newton-like Method for Molecular Mechanics Energy Minimization of Large Molecules. *J. Comput. Chem.* **1987**, *8*, 1016−1024.

https://doi.org/10.1021/acs.jpcb.3c06433
J. Phys. Chem. B 2023, 127, 10871−10879